Binary crystals in two-dimensional two-component Yukawa mixtures

Lahcen Assoud, René Messina,[a] and Hartmut Löwen
Institut für Theoretische Physik II: Weiche Materie, Heinrich-Heine-Universität Düsseldorf, Universitätsstrasse 1, D-40225 Düsseldorf, Germany

(Received 18 April 2008; accepted 11 September 2008; published online 28 October 2008)

The zero-temperature phase diagram of binary mixtures of like-charge particles interacting via a screened Coulomb pair potential is calculated as a function of composition and charge ratio. The potential energy obtained by a Lekner summation is minimized among a variety of candidate two-dimensional crystals. A wealth of different stable crystal structures is identified including A, B, AB_2, A_2B, and AB_4 structures [A (B) particles correspond to large (small) charge.] Their elementary cells consist of triangular, square, or rhombic lattices of the A particles with a basis comprising various structures of A and B particles. For small charge asymmetry there are no intermediate crystals besides the pure A and B triangular crystals. The predicted structures are detectable in experiments on confined mixtures of like-charge colloids or dusty plasma sheets. © *2008 American Institute of Physics*. [DOI: 10.1063/1.2996515]

I. INTRODUCTION

Two-component mixtures in general exhibit much richer crystallization phenomena and polymorphism than their one-component counterparts[1] as witnessed by a huge variety of possible stable binary crystals, e.g., for binary hard sphere systems.[2–5] How the whole crystal phase behavior in mixtures depends on the interparticle interactions is far from being understood even in equilibrium.[6,7] This is true also in two spatial dimensions where the number of Bravais lattices is smaller than in three dimensions. Binary mixtures in two dimensions have been studied for hard disks[8] and a complex diagram of close packing was obtained as a function of their diameter ratio. More recently, a two-dimensional binary mixture with soft interactions was considered,[9] namely that for parallel dipoles where the pair potential scales with the inverse cube of the interparticle separation. A variant of this model has been considered in Ref. 10. Such systems can be realized in granular matter[11] and in magnetic colloidal suspensions confined to an air-water interface.[12] Again, as a function of the ratio of dipole moments of the two species, a complex phase diagram of stable binary crystals was obtained that qualitatively differs from the hard disk case.[8] In particular for low asymmetries, the hard disk system shows a complete separation into pure A and B triangular crystals[8] while the soft dipolar systems possesses two stable mixed crystals as well with stoichiometric ratio A_2B and AB_2.[9] These differences show that the topology of the phase diagrams depends on details of the interactions and there is certainly a need to understand this dependence in more detail.

In this paper, we consider a two-dimensional binary system of Yukawa pointlike particles, i.e., the pair interaction potential $V(r)$ between the particles is a screened Coulomb interaction $\propto \exp(-\kappa r)/r$ where κ is the screening constant (or the inverse screening length). This repulsive potential interpolates between the case of hard disks (as obtained in the limit of high κ) and the unscreened Coulomb case (as obtained for $\kappa=0$). The latter limit, $V(r) \propto 1/r$ is even softer than the dipolar case where $V(r) \propto 1/r^3$. The two components are defined by two different charges, i.e., different prefactors in front of the Yukawa interaction. In previous works, such classical binary mixture with Yukawa interactions in three dimensions has been used as a model to study mixing rules,[13] effective forces,[14] fluid-fluid phase separation,[15–17] dynamical correlations,[18,19] and transport properties.[20] Likewise the pure (one-component) Yukawa system was also studied in two-spatial dimensions for fluid structure,[21–24] dynamics,[25–28] and transport properties.[29] Binary mixtures of Yukawa particles in two dimensions have also been studied for fluid structure,[30] adsorption,[31] interfaces,[32] and transport.[33]

The Yukawa potential is a good description for an effective pair interaction in *charged colloidal suspensions*[34] and in *dusty plasmas*,[35] both for one component systems and mixtures. Here the microions establish a responding neutralizing background and they only enter via a Debye screening length and any microscopic details (as manifested, e.g., in the Hofmeister series) are neglected. In fact, highly charged colloidal suspensions can be confined between highly charged parallel glass plates,[36–38] which restricts their motion practically to two dimensions. As in three dimensions, the Debye–Hückel screened Coulomb interaction is a reasonable model for confined charged colloids.[39,40] Crystallization of binary charged colloids has been studied experimentally in the bulk. For instance, the phase diagram for oppositely charged colloids can be found in Refs. 41 and 42. A crystalline monolayer has also been realized experimentally for a confined binary mixture of like-charged colloids (see Fig. 1 in Ref. 43).[44] Similar studies exist also for sterically stabilized[45] and magnetic colloids.[46] On the other hand, sheets of highly charged dust particles in plasmas (so-called complex plasmas) can also be confined to two dimensions, e.g., by levitating electric fields. The interaction between the dust particles is again screened such that a Yukawa model is

[a]Electronic mail: messina@thphy.uni-duesseldorf.de.

appropriate.[35,47,48] Highly charged microspheres suspended in a plasma settled in a horizontal monolayer were studied experimentally and compared to a two-dimensional Yukawa model.[49–51] There is no principle problem in studying binary mixtures of dust particles but a concrete realization in experiments still has to be performed as well. Finally, another possible realization of the binary charged Yukawa system might be in two-component Langmuir–Blodgett films.[52–54]

Apart from its important realizations, the major motivation for our studies is to understand the interplay between the interparticle interaction and the stability of different two-dimensional crystal lattices. A control of colloidal composite lattices may lead to new photonic crystals[55] to molecular sieves[56] and to micro- and nanofilters with desired porosity.[57] The electric properties of a nanocrystal depend on its superlattice structure.[58] For these type of applications, it is crucial to understand the various stable lattice types in binary mixtures.

For the two-component two-dimensional Yukawa mixture, we obtain the full phase diagram at zero-temperature as a function of the charge asymmetry using lattice sums. As a result, we find a variety of different stable composite lattices. They include A, B, AB_2, A_2B, and AB_4 structures. Their elementary cells consist of (equilateral) triangular, square, and rhombic lattices of the big particles. These are highly decorated by a basis involving either A particles alone or both B and A particles. The topology of the resulting phase diagram differs qualitatively from that of hard disk mixtures[8] and dipoles.[9]

The paper is organized as follows: In Sec. II the model is described and possible candidate structures for crystal lattices in two dimensions are proposed. Results for the thermodynamics and for the phase diagrams are presented in Sec. III. We conclude finally in Sec. IV.

II. MODEL

The model used in our study is a binary mixture of (repulsive) charged particles made up of two species denoted as A and B. Each component A and B is characterized by its charge valency Z_A and Z_B, respectively. These point particles are confined to a two-dimensional plane and interact via a Yukawa pair potential. Introducing the charge ratio $Z=Z_B/Z_A$,[59] the pair interaction potentials between two A-particles, an A- and a B-particle, and two B-particles at distance r are

$$V_{AA}(r)=\kappa V_0\varphi(r),\quad V_{AB}(r)=\kappa V_0 Z\varphi(r),\quad V_{BB}(r)=\kappa V_0 Z^2\varphi(r), \tag{1}$$

respectively. The dimensionless function $\varphi(r)$ is given by

$$\varphi(r)=\frac{\exp(-\kappa r)}{\kappa r}, \tag{2}$$

where the energy amplitude $V_0\kappa$ sets the energy scale. In Debye–Hückel theory, the prefactor reads as $V_0=Z_A^2/\epsilon$ where ϵ is the dielectric permittivity of the solvent ($\epsilon=1$ for the dusty plasma). Typically,[60,61] Z_A is on the order of 100–100 000 elementary charges e such that $V(r)/k_BT$ at typical interparticle distances $r=1/\kappa$ equals $Z_A^2\kappa\lambda_B/e^2$. Typically, the Bjerrum length $\lambda_B=e^2/\epsilon k_BT$ is a few angstroms at room temperature and the Debye screening length $1/\kappa$ is 1 μm, such that $V(r)/k_BT$ is much larger than unity for high charges Z_A. This justifies formally zero-temperature calculations for the Yukawa particles. On the other hand, the screening microions possess a finite temperature, which enters in the inverse Debye screening length κ.

Our goal is to determine the stable crystalline structures adopted by the system at zero temperature. We consider a parallelogram as a primitive cell, which contains n_A A-particles and n_B B-particles. This cell can be described geometrically by the two lattice vectors $\mathbf{a}=a(1,0)$ and $\mathbf{b}=a\gamma(\cos\theta,\sin\theta)$, where θ is the angle between $\mathbf{a}$ and $\mathbf{b}$ and γ is the aspect ratio ($\gamma=|\mathbf{b}|/|\mathbf{a}|$). The position of a particle i (of species A) and that of a particle j (of species B) in the parallelogram is specified by the vectors $\mathbf{r}_i^A=(x_i^A,y_i^A)$ and $\mathbf{r}_j^B=(x_j^B,y_j^B)$, respectively. The total internal energy (per primitive cell) U has the form

$$U=\frac{1}{2}\sum_{J=A,B}\sum_{i,j=1}^{n_J}{}'\sum_{\mathbf{R}}V_{JJ}(|\mathbf{r}_i^J-\mathbf{r}_j^J+\mathbf{R}|)+\sum_{i=1}^{n_A}\sum_{j=1}^{n_B}\sum_{\mathbf{R}}V_{AB}(|\mathbf{r}_i^A-\mathbf{r}_j^B+\mathbf{R}|), \tag{3}$$

where $\mathbf{R}=k\mathbf{a}+l\mathbf{b}$ with k and l being integers. The sums over $\mathbf{R}$ in Eq. (3) run over all lattice cells where the prime indicates that for $\mathbf{R}=0$ the terms with $i=j$ are to be omitted. In order to handle efficiently the long-range nature of the Yukawa interaction at moderate screening strength, we employed a Lekner summation (see Appendix).

We choose to work at prescribed pressure[62] p and zero temperature ($T=0$). Hence, the corresponding thermodynamic potential is the Gibbs free energy G. Additionally, we consider interacting particles at composition $X:=n_B/(n_A+n_B)$, so that the (intensive) Gibbs free energy g per particle reads: $g=g(p,Z,X)=G/(n_A+n_B)$. At vanishing temperature, g is related to the internal energy per particle $u=U/(n_A+n_B)$ through $g=u+p/\rho$, where the pressure p is given by $p=\rho^2(\partial u/\partial\rho)|_{n_A,n_B}$, and $\rho=(n_A+n_B)/|\mathbf{a}\times\mathbf{b}|$ is the total particle density. The Gibbs free energy per particle g has been minimized with respect to γ, θ, and the position of particles of species A and B within the primitive cell. In order to decrease the complexity of the energy landscape, we have limited the number of variables and considered the following candidates for our binary mixtures: A_4B, A_3B, A_2B, A_4B_2, A_3B_2, AB, A_2B_2, A_3B_3, A_2B_3, AB_2, A_2B_4, AB_3, AB_4, and AB_6. Note that crystalline alloys with chemical disorder which are stable due to mixing entropy are not considered here since our study is limited to zero temperature. For the AB_6 and A_3B_3 case we have only considered a triangular lattice formed by the A particles. An overview of the resulting stable crystalline phases can be found in Fig. 1. The corresponding nomenclature of the phase labeling is summarized and explained in Table I. The crystalline structures are getting increasingly complex from top to bottom in Fig. 1 and Table I. Pure triangular lattices [$\mathbf{T}(A)$ or $\mathbf{T}(B)$] and checker-

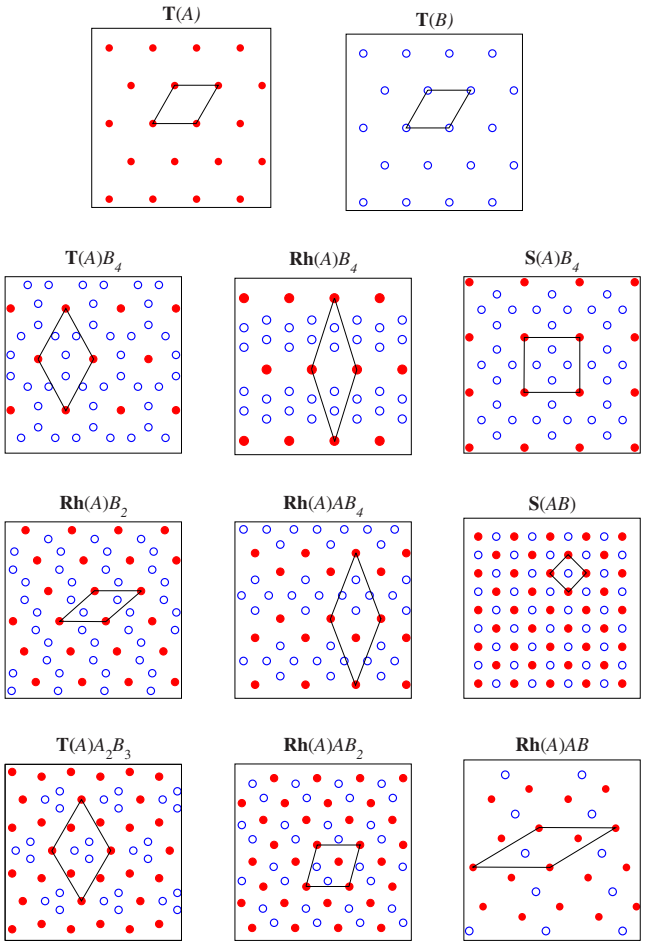

FIG. 1. (Color online) The stable binary crystal structures and their primitive cells. The disks (open circles) correspond to A (B) particles.

board structures with equal molarities [$\mathbf{S}(AB)$] are the simpler structures while more complex basic unit cells with a complicated basis are included as well.

III. RESULTS

A. Thermodynamical properties

1. Gibbs free energy

We first would like to address the behavior of the reduced Gibbs free energy per particle $g^* \equiv g/(V_0\kappa)$ at prescribed charge ratio Z. The (*discrete*) profiles of g^* for different values of Z as a function of the composition X are depicted in Fig. 2. The different data points shown in Fig. 2 correspond to the phase (see Table II) with the lowest energy at given composition and charge ratio. This does not necessarily imply that this particular phase is globally stable, see our discussion below. The qualitative trends of g^* are not affected upon varying the pressure. In the following we introduce a reduced pressure $p^* = p/(V_0\kappa^3)$.

TABLE I. The stable phases with their Bravais lattice and their basis.

Phase	Bravais lattice [basis]
$\mathbf{T}(A)$	Triangular for A [one A particle]
$\mathbf{T}(B)$	Triangular for B [one B particle]
$\mathbf{S}(AB)$	Square for A and B together [one A and one B particles]
$\mathbf{S}(A)B_n$	Square for A [one A and n B particles]
$\mathbf{Rh}(A)A_mB_n$	Rhombic for A [$(m+1)$ A and n B particles]
$\mathbf{T}(A)A_mB_n$	Triangular for A [$(m+1)$ A and n B particles]

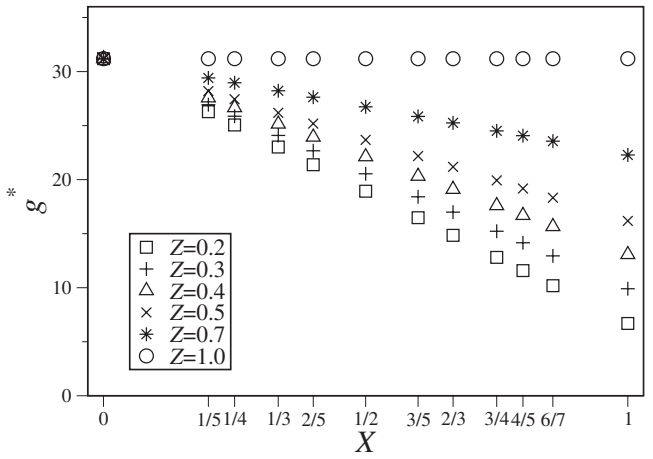

FIG. 2. Reduced Gibbs free energy g^* as a function of the composition X for various charge ratios Z at prescribed reduced pressure $p^*=100$. The different data points shown correspond to the phase with the lowest energy at given composition and charge ratio. The case $Z=1$ corresponds to the pure phase $\mathbf{T}(A)$ (or equivalently $\mathbf{T}(B)$). All the other phases are gathered in Table II.

At a given composition X, Fig. 2 shows that g^* decreases with decreasing charge ratio Z. Recalling that $g^* = u^* + p^*/\rho^*$ [with $u^* \equiv u/(V_0\kappa)$], this feature can be discussed in terms of u^* and ρ^*. More precisely, at a prescribed value for X, the system has to lower its density such as to keep the pressure constant when Z is enlarged. This clearly explains why the term in p^*/ρ^* increases here with growing Z at fixed X. What is less straightforward to clarify is the resulting behavior of u^* (with respect to Z and ρ^*), which can only be specified after the explicit numerical calculations.

The other general trend revealed in Fig. 2 is that g^* decreases with growing composition X at prescribed charge ratio Z. This feature is fully consistent with the idea that upon enlarging X, the proportion of *weakly* charged B-particles increases accordingly, so that to keep the pressure constant the system has to increase its density and therefore the term $1/\rho^*$ in g^* decreases. Again, the behavior of u^* is not trivial a priori.

2. Phase coexistence

In this part, we explain how a phase coexistence sets in. The onset of phase coexistence is based on the common tangent construction also called Maxwell construction. At coexistence, two conditions must be fulfilled: (i) the pressure p^* needs to be equal for each phase (in our situation this is always guaranteed since we are working at prescribed pressure) and (ii) the chemical potential for any component must be the same for the two coexisting phases. If we denote by $\mu_i^{\pi_j}$, with $i=A,B$ and $j=1,2$ the chemical potential associated to particles of i-species for phase π_j, then the thermodynamical condition (ii) can be mathematically expressed as: $\mu_A^{\pi_1} = \mu_A^{\pi_2}$ and $\mu_B^{\pi_1} = \mu_B^{\pi_2}$.

The geometrical interpretation of this latter thermodynamical condition combined with that of the minimization of

TABLE II. The phases with the lowest Gibbs free energy g^* appearing in Fig. 2. The labels **Re** and **Pa** correspond to rectangular and parallelogram shaped primitive cells.

X Z	0.2	0.3	0.4	0.5	0.7
0	**T**(A)	**T**(A)	**T**(A)	**T**(A)	**T**(A)
1/5	**Rh**$(A)A_3B$	**Rh**$(A)A_3B$	**Rh**$(A)A_3B$	**Rh**$(A)A_3B$	**Rh**$(A)A_3B$
1/4	**Re**$(A)A_2B$	**Re**$(A)A_2B$	**Re**$(A)A_2B$	**Re**$(A)A_2B$	**Re**$(A)A_2B$
1/3	**Rh**$(A)AB$	**Re**$(A)A_3B_2$	**Pa**$(A)A_3B_2$	**Pa**$(A)A_3B_2$	**T**(A_2B)
2/5	**Rh**$(A)A_2B_2$	**Re**$(A)A_2B_2$	**Pa**$(A)A_2B_2$	**Pa**$(A)A_2B_2$	**Rh**$(A)A_2B_2$
1/2	**S**(AB)	**Rh**$(A)AB_2$	**Rh**$(A)AB_2$	**Rh**$(A)AB_2$	**Re**$(A)AB_2$
3/5	**Re**$(A)AB_3$	**Re**$(A)AB_3$	**Pa**$(A)AB_3$	**Pa**$(A)AB_3$	**Rh**$(A)AB_3$
2/3	**Rh**$(A)AB_2$	**Rh**$(A)AB_2$	**Rh**$(A)AB_4$	**Rh**$(A)AB_4$	**T**(AB_2)
3/4	**Pa**$(A)B_3$	**Re**$(A)B_3$	**Re**$(A)B_3$	**Re**$(A)B_3$	**Re**$(A)B_3$
4/5	**T**$(A)B_4$	**Rh**$(A)B_4$	**S**$(A)B_4$	**S**$(A)B_4$	**Rh**$(A)B_4$
6/7	**T**$(A)B_6$	**T**$(A)B_6$	**T**$(A)B_6$	**T**$(A)B_6$	**T**$(A)B_6$
1	**T**(B)	**T**(B)	**T**(B)	**T**(B)	**T**(B)

g^* is exemplified in Fig. 3. Thereby, we have plotted $\Delta g^*(X)=g^*(X)-[(1-X)g_A^*+Xg_B^*]$, where $g_A^*=g^*(X=0)$ and $g_B^*=g^*(X=1)$. The common tangent construction for crystalline phases consists merely of excluding all metastable phases in the discrete profile of $\Delta g^*(X)$. For the examples chosen in Fig. 3 it turns out that for $Z=0.7$ all mixtures are unstable so that the resulting equilibrium system will always split into a pure A and pure B triangular crystals. On the other hand, when $Z=0.3$, three stable mixtures for $X=1/2$, 2/3, and 4/5 set in, which are explicitly mentioned in Fig. 3. They are all hit by the two double tangents. In total, there are four pieces of common tangents shown in Fig. 3 (lower part) for $Z=0.3$ as a dashed line.

3. Particle density

The reduced density ρ^* as a function of the charge ratio Z at different compositions X is sketched in Fig. 4. At given composition X, the density decreases monotonically with Z, see Fig. 4. This effect can be simply explained as follows: Upon increasing Z the repulsive A-B and B-B pair interactions increase accordingly, so that to keep the pressure fixed the system has to decrease its density. Moreover, at prescribed charge ratio, Fig. 4 indicates that the density increases with the composition. This feature can also be explained with simple physics: Upon enlarging the composition X, the proportion of weakly charged B-particles increases accordingly, so that to keep the pressure constant the system has to increase its density. This particle density behavior is important to better understand later the phase diagram which is shown for prescribed pressure.

B. Phase diagram

The ultimate phase diagrams in the (Z,X) plane has been obtained by employing the Maxwell construction. To allow an easier comparison with earlier works,[8,9] we have chosen the same y-axis, namely here the composition X. We recall here that both dimensionless quantities, namely the charge ratio Z as well as the composition X, can vary between zero and unity. A low charge ratio (i.e., Z is close to zero) indicates a strong charge asymmetry, whereas a high charge ratio (i.e., Z is close to unity) represents a large charge symmetry or equivalently a weak charge asymmetry. Given the fact that the phase behavior is getting increasingly complicated upon lowering Z, involving a huge basket of candidates, we only present results starting from $Z=0.2$. Furthermore, in contrast to situations where the pair potential can be described as a power law of the separation distance (as it was the case in

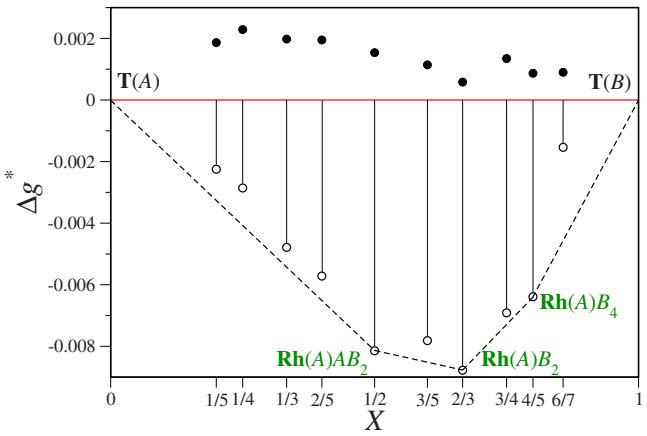

FIG. 3. (Color online) Common tangent construction for crystalline phases at prescribed reduced pressure $p^*=100$. The filled (open) circles correspond to $Z=0.7$ ($Z=0.3$). The stable phases are indicated explicitly.

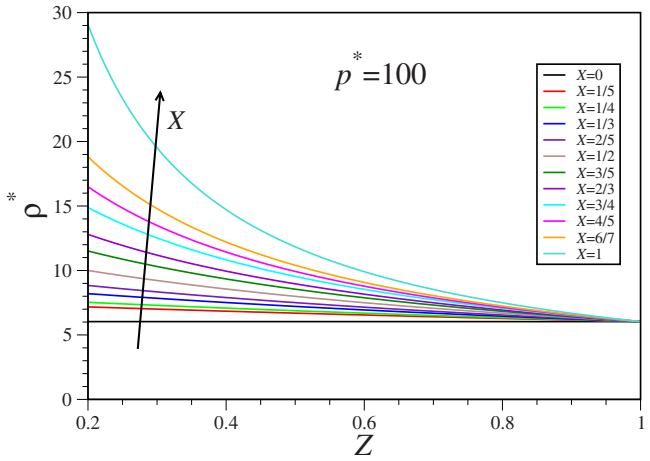

FIG. 4. (Color online) Reduced density ρ^* (prior the Maxwell construction) as a function of the charge ratio Z for various compositions X at prescribed reduced pressure $p^*=100$. The arrow indicates growing X.

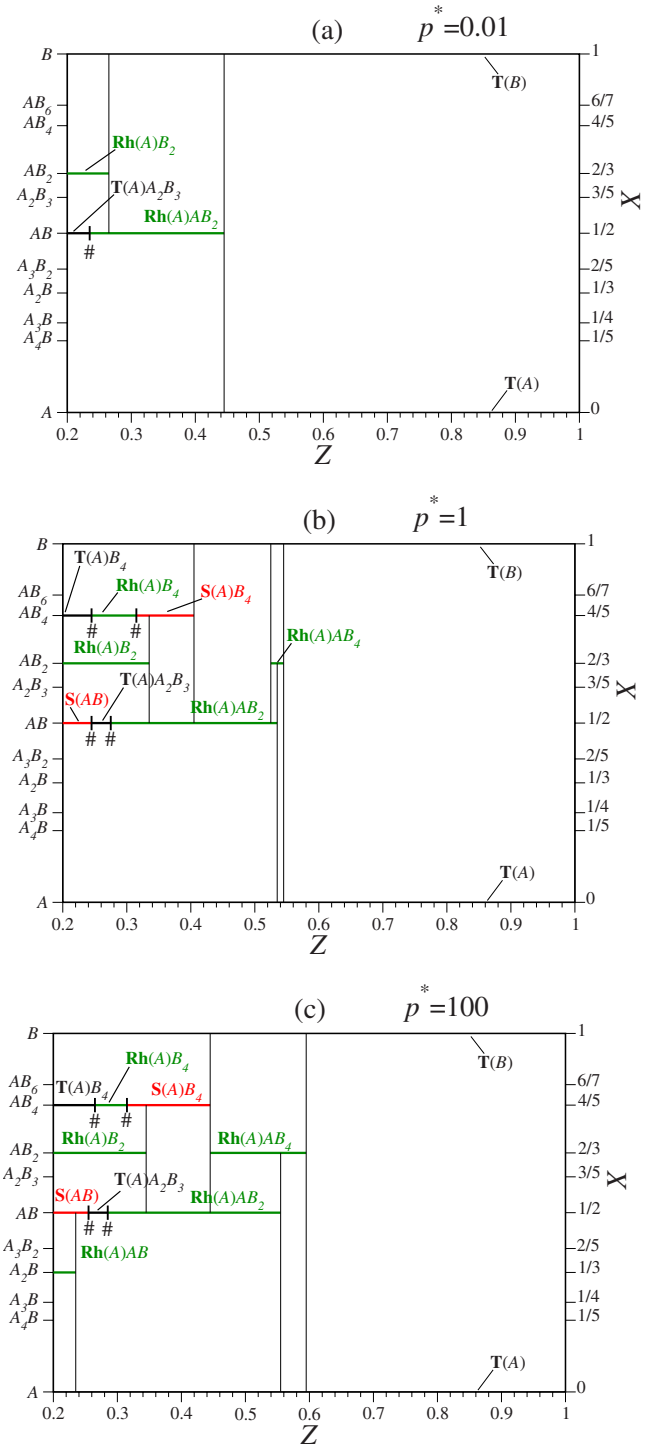

FIG. 5. (Color online) The phase diagram in the (Z,X) plane of charge asymmetry and composition at $T=0$ for an effective pressure (a) $p^*=0.01$, (b) $p^*=1$, (c) $p^*=100$. The symbol # denotes a discontinuous transition. The y-axis is represented by two equivalent scales: The left side indicates the phase symbols whereas the right one shows the corresponding value of the composition.

our previous work on dipolar mixtures[9]), the phase diagram becomes pressure dependent for Yukawa systems. To capture this feature, we present results at three well distinct pressures, namely $p^* \equiv p/(V_0\kappa^3)=0.01$, 1, and 100.

The phase diagrams in the (Z,X) plane for the three reduced pressures $p^*=0.01$, 1, and 100 are depicted in Figs. 5(a)–5(c), respectively.

1. Weak charge asymmetry

Let us first focus our discussion on the apparently simple phase behavior reported at weak charge asymmetry (here roughly $Z \gtrsim 0.5$, see Fig. 5). Thereby, the system phase separates into a pure A and a pure B triangular crystalline phase (see also Fig. 1). This triangular structure obviously corresponds to the single-component ground state.

What is now less obvious, still in the regime of weak charge asymmetry, is the phase separation reported in Fig. 5(c) for $p^*=100$. Recently, we have shown for dipolar binary mixtures,[9] whose pair potential is governed by $1/r^3$, that, at weak dipolar asymmetry (the analogous quantity to the charge ratio in our present study), the *stable mixtures* A_2B and AB_2 (who are globally triangular) set in. This phase behavior contrasts therefore strongly with that reported here for Yukawa mixtures, see Fig. 5(c). Given the fact that at weak screening the Yukawa pair potential is well approximated by a $1/r$ dependence, which is even softer than $1/r^3$, it is legitimate to expect stable mixtures in the regime of weak screening and charge asymmetry. In order to check this idea we have performed additional calculations at $p^*=10^{10}$ with $Z=0.99$ leading to reduced screening strengths of the order of 10^{-2}. Those values for κ^* turn out to be still too large to recover the phase behavior found at $1/r^3$-pair interactions.[9] The consideration of even much smaller screening strengths (say roughly of the order of 10^{-7}) are numerically not tractable within reasonable CPU time. Unfortunately, the implementation of a direct Lekner and/or Ewald sum for the $1/r$-pair interactions is delicate at *prescribed pressure*, since the lack of electroneutrality involves the presence of an artificial homogeneous neutralizing background which is thermodynamically only consistent at *prescribed density*.[63] Consequently, although we have a strong intuition about the stability of mixtures at weak charge asymmetry and screening, we cannot prove it here on computational basis.

2. Large charge asymmetry

We now address the more complicated phase behavior reported at strong charge asymmetry, see Fig. 5 with $Z \lesssim 0.5$. As a clear general trend, it is found that the number of stable phases increases with growing pressure. This feature is in agreement with the idea that mixing is favored upon softening the pair potential.

A common and remarkable feature in this regime of strong charge asymmetry (see Fig. 5) is the imposing stability of equal composition $X=1/2$. This feature was also reported for dipolar mixtures.[9] Let us discuss the behavior at $X=1/2$ in more detail. In fact, the following cascade $\mathbf{S}(AB) \rightarrow \mathbf{T}(A)A_2B_3 \rightarrow \mathbf{R}h(A)AB_2$ is found upon increasing Z, see Fig. 5 and Fig. 1 for the corresponding structures. Thereby, the transitions $\mathbf{S}(AB) \rightarrow \mathbf{T}(A)A_2B_3$ and $\mathbf{T}(A)A_2B_3 \rightarrow \mathbf{R}h(A)AB_2$ are discontinuous, see Fig. 5. These discontinuous transitions stem merely from the lattice-geometry incompatibility among the phases, see Fig. 1. Note that, for $p^*=0.01$ shown in Fig. 5(a), the stability of the square phase $\mathbf{S}(AB)$ occurs for values of Z smaller than 0.2 that are not shown here.

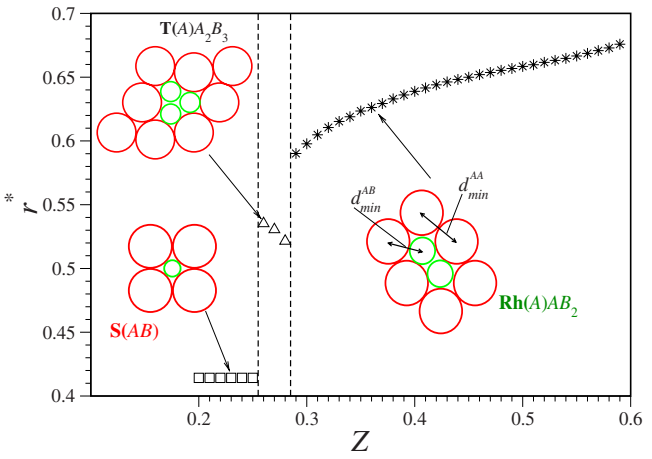

FIG. 6. (Color online) Geometrical order parameter $r^*=(2d^{AB}_{\min}-d^{AA}_{\min})/d^{AA}_{\min}$ as a function of the charge ratio Z for the given composition $X=1/2$ at prescribed reduced pressure $p^*=100$. The equivalent stable hard disk systems are sketched as well as the distances $d^{AB}_{\min}$ and $d^{AA}_{\min}$ for the $\mathbf{Rh}(A)AB_2$ phase.

In order to compare the phase behavior with that of hard disk mixtures, we have considered the following dimensionless geometrical order parameter:

$$r^* \equiv \frac{2d^{AB}_{\min} - d^{AA}_{\min}}{d^{AA}_{\min}} (r \leq 1), \tag{4}$$

where $d^{AB}_{\min}$ corresponds to the shortest distance between A-and B-particles whereas $d^{AA}_{\min}$ stands for that between A-particles within the Wigner–Seitz cell (see Fig. 6). Physically, this quantity r^* is the size ratio between big and small particles in a (packed) binary hard disk crystal,[8] i.e., for touching configurations. The profile of r^* along the cascade $\mathbf{S}(AB) \rightarrow \mathbf{T}(A)A_2B_3 \rightarrow \mathbf{Rh}(A)AB_2$ depicted in Fig. 5(c) is sketched in Fig. 6 as a function of Z. As expected, r^* undergoes two jumps at $Z=0.255$ and $Z=0.285$, which are the signatures of discontinuous transitions. Figure 6 reveals that r^* is *growing* with Z except for the tiny interval where the $\mathbf{T}(A)A_2B_3$ phase is stable. This demonstrates an interesting analogy between the charge ratio Z in like-charged binary mixtures and the size ratio r^* in hard disk binary mixtures consistent with earlier investigations where size polydispersity was mapped onto charge polydispersity[64] and a strong correlation between size and charge polydispersity was found. In fact, for hard-disk mixtures there is also a first-order transition from the $\mathbf{S}(AB)$ directly to the $\mathbf{Rh}(A)AB_2$ phase at a size asymmetry between 0.4 and 0.5.[8] This is the analogy of the start and end of the cascade $\mathbf{S}(AB) \rightarrow \mathbf{T}(A)A_2B_3 \rightarrow \mathbf{Rh}(A)AB_2$. It is interesting that the hard-disk transition occurs at similar size asymmetries as indicated on the y axis of Fig. 6. However, in our case, the additional structure $\mathbf{T}(A)A_2B_3$ (with a decreasing r^*) intervenes.

IV. CONCLUDING REMARKS

In conclusion we have determined the ground-state (i.e., zero-temperature) phase diagram for a two-component Yukawa monolayer at various pressures for arbitrary compositions and a broad range of charge asymmetries. Among a big number of candidate phases, a wealth of different composite lattices has been found to be stable. The larger the charge asymmetry, the more complex is the phase diagram. At low asymmetry the system shows demixing into pure A and B crystals similar to hard disks but different from the soft inverse cube interaction valid for dipoles. At higher asymmetries and same composition of high-charge and low-charge particles, there are two first-order transitions between three different crystalline structures with incompatible symmetry. The latter transitions were compared with the corresponding hard-disk behavior. The results are in principle detectable in binary mixtures of charged colloids confined between two charged plates[43] or levitated dusty plasma sheets.[65]

It would be interesting to study the effect of finite temperature. We expect that the topology of the phase diagram does not change upon gently increasing the temperature though this could change close to melting. In this respect, colloid-polymer mixtures are useful model systems where the concentration of nonadsorbing polymers plays the role of inverse temperature, see e.g., Refs. 66 and 67.

When cooling a two-component fluid down, glass formation in the binary systems at finite temperature may be a fascinating topic as well[68] to be studied in the future. In fact, it has been speculated that the underlying crystallization into the stable crystal lattices may control vitrification[69] and therefore our findings are directly relevant for the structure of glasses.

ACKNOWLEDGMENTS

We thank T. Palberg and H. Tanaka for helpful discussions. This work was supported by the DFG via the SFB TR6 (project D1).

APPENDIX: LEKNER SUMS FOR YUKAWA INTERACTIONS IN TWO DIMENSIONAL SYSTEMS

We consider a primitive cell in the shape of a parallelogram, which contains a set of $n=n_A+n_B$ particles interacting via Yukawa potentials. The parallelogram repeated in the xy plane gives a two-dimensional lattice and can be described by two lattice vectors $\mathbf{a}=(a_x,0)$ and $\mathbf{b}=(b_x,b_y)$. In the parallelogram, the position of a charge valency Z_i is defined by $\mathbf{r}_i=(x_i,y_i)$.

The total interaction energy per cell is given by

$$\frac{U}{V_0} = \frac{1}{2}\sum_{i=1}^{n}\sum_{j\neq 1}^{n} Z_i Z_j \Phi(\mathbf{r}_{ij}) + \frac{1}{2}\sum_{i=1}^{n} Z_i^2 \Phi_0 \tag{A1}$$

with

$$\Phi(\mathbf{r}) = \sum_{\mathbf{R}} \frac{\exp(-\kappa|\mathbf{r}+\mathbf{R}|)}{|\mathbf{r}+\mathbf{R}|} \tag{A2}$$

and

$$\Phi_0 = \sum_{\mathbf{R}\neq 0} \frac{\exp(-\kappa|\mathbf{R}|)}{|\mathbf{R}|},$$

where

$$|\mathbf{r}+\mathbf{R}| = \sqrt{(x+a_x l+b_x m)^2+(y+b_y m)^2}$$

and

$$|\mathbf{R}| = \sqrt{(a_x l+b_x m)^2+(b_y m)^2}.$$

Here $\mathbf{R}=l\mathbf{a}+m\mathbf{b}$ with l and m being integers. The slowly convergent sums over lattice sites [Eq. (A2)] cannot be efficiently used in a numerical calculation, so that we will transform them into rapidly convergent forms using a Lekner method.[70,71] With the help of the following integral representation

$$\frac{\exp(-\kappa|\mathbf{r}+\mathbf{R}|)}{|\mathbf{r}+\mathbf{R}|} = \frac{1}{\sqrt{\pi}}\int_0^\infty \frac{dt}{\sqrt{t}}\exp\left(-\frac{\kappa^2}{4t}-|\mathbf{r}+\mathbf{R}|^2 t\right), \tag{A3}$$

we obtain

$$\Phi(\mathbf{r}) = \frac{1}{\sqrt{\pi}}\int_0^\infty \frac{dt}{\sqrt{t}}\left\{\exp\left(-\frac{\kappa^2}{4t}\right)\sum_{m=-\infty}^{\infty}\sum_{l=-\infty}^{\infty}\exp[-(y+mb_y)^2 t] \times\exp\left[-\left(\frac{x}{a_x}+l+m\frac{b_x}{a_x}\right)^2 a_x^2 t\right]\right\}. \tag{A4}$$

Now, to get further, we apply a one-dimensional Poisson summation

$$\sum_{l=-\infty}^{\infty}\exp[-(\alpha+\beta l)^2 t] = \frac{\sqrt{\pi}}{\beta\sqrt{t}}\sum_{k=-\infty}^{\infty}\exp\left(i2\pi k\frac{\alpha}{\beta}\right)\exp\left(-\frac{\pi^2 k^2}{\beta^2}\frac{1}{t}\right), \tag{A5}$$

which provides

$$\sum_{l=-\infty}^{+\infty}\exp\left[-\left(\frac{x}{a_x}+l+m\frac{b_x}{a_x}\right)^2 a_x^2 t\right] = \frac{1}{|a_x|}\sqrt{\frac{\pi}{t}}\left[1+2\sum_{k=1}^{+\infty}\cos\left[2\pi k\left(\frac{x}{a_x}+m\frac{b_x}{a_x}\right)\right] \times\exp(-\pi^2 k^2/a_x^2 t)\right]. \tag{A6}$$

Inserting Eq. (A6) into Eq. (A4) yields:

$$\Phi(\mathbf{r}) = \frac{1}{|a_x|}\sum_{m=-\infty}^{\infty}\int_0^\infty \frac{dt}{t}\exp\left[-\frac{\kappa^2}{4t}-(y+mb_y)^2 t\right] + \frac{2}{|a_x|}\sum_{k=1}^{+\infty}\sum_{m=-\infty}^{+\infty}\cos\left[2\pi k\left(\frac{x}{a_x}+m\frac{b_x}{a_x}\right)\right] \times\int_0^\infty \frac{dt}{t}\exp\left[-\left(\kappa^2+\frac{4\pi^2 k^2}{a_x^2}\right)\frac{1}{4t}-(y+mb_y)^2 t\right]. \tag{A7}$$

Now, taking into account the following relation

$$\int_0^\infty \frac{dt}{t}\exp\left(-\frac{B^2}{4t}-C^2 t\right) = 2K_0(BC), \tag{A8}$$

where K_0 is the zeroth order modified Bessel function of the second kind. The final expression for $\Phi(\mathbf{r})$ reads:

$$\Phi(\mathbf{r}) = \frac{2}{|a_x|}\sum_{m=-\infty}^{+\infty}K_0(\kappa|y+mb_y|) + \frac{4}{|a_x|}\sum_{k=1}^{\infty}\sum_{m=-\infty}^{+\infty}\cos\left[2\pi\left(\frac{x}{a_x}+m\frac{bx}{a_x}\right)\right] \times K_0\left[|y+mb_y|\sqrt{\kappa^2+\frac{4\pi^2 k^2}{a_x^2}}\right] \quad \text{for} \quad y\neq 0 \tag{A9}$$

and the "self" contribution Φ_0

$$\Phi_0 = \frac{4}{|a_x|}\sum_{m=1}^{\infty}K_0(\kappa m b_y)+\frac{8}{|a_x|}\sum_{k=1}^{\infty}\sum_{m=1}^{\infty}\cos\left(2\pi k m\frac{bx}{a_x}\right) \times K_0\left[mb_y\sqrt{\kappa^2+\frac{4\pi^2 k^2}{a_x^2}}\right] - \frac{2}{|a_x|}\ln[1-\exp(-\kappa a_x)]. \tag{A10}$$

In the limit of a rectangular based cell, i.e., setting $b_x=0$, one obtains the formulas for the cross and self-energies that are identical to those derived in Ref. 71 with $z=0$.

The sums in Eqs. (A9) and (A10) are truncated (i.e., the criterion of convergence is realized) when the Bessel function values are smaller than 10^{-12}. This typically leads to a relative error in the energy that is smaller than 10^{-11}. In the case of double sums the cutoffs are identical, i.e., $k_c=m_c$, such that all terms with $k\leq k_c$ and $|m|\leq m_c$ are included in the sums.

[1] G. Tammann, Ann. Phys. **40**, 297 (1913).
[2] S. Pronk and D. Frenkel, Phys. Rev. Lett. **90**, 255501 (2003).
[3] H. Xu and M. Baus, J. Phys.: Condens. Matter **4**, L663 (1992).
[4] M. D. Eldridge, P. A. Madden, and D. Frenkel, Nature (London) **365**, 35 (1993).
[5] P. Bartlett, R. H. Ottewill, and P. N. Pusey, Phys. Rev. Lett. **68**, 3801 (1992).
[6] J. Hafner, *From Hamiltonians to Phase Diagrams* (Springer, Berlin, 1987).
[7] G. Gompper and M. Schick, in *Soft Matter*, Complex Colloidal Suspensions Vol. 2 (Wiley, Weinheim, 2006).
[8] C. N. Likos and C. L. Henley, Philos. Mag. B **68**, 85 (1993).
[9] L. Assoud, R. Messina, and H. Löwen, Europhys. Lett. **80**, 48001 (2007).
[10] J. Fornleitner, F. Lo Verso, G. Kahl, and C. N. Likos, Soft Matter **4**, 480 (2008).
[11] M. B. Hay, R. K. Workman, and S. Manne, Phys. Rev. E **67**, 012401 (2003).
[12] K. Zahn, J. M. MendezAlcaraz, and G. Maret, Phys. Rev. Lett. **79**, 175 (1997).
[13] Y. Rosenfeld, Phys. Rev. E **47**, 2676 (1993).
[14] A. A. Louis, E. Allahyarov, H. Löwen, and R. Roth, Phys. Rev. E **65**, 061407 (2002).
[15] E. Scholl-Paschinger and G. Kahl, J. Chem. Phys. **118**, 7414 (2003).
[16] P. Hopkins, A. J. Archer, and R. Evans, J. Chem. Phys. **124**, 054503 (2006).
[17] J. Köfinger, N. B. Wilding, and G. Kahl, J. Chem. Phys. **125**, 234503

(2006).
[18] M. A. Chavez-Rojo and M. Medina-Noyola, Physica A **366**, 55 (2006).
[19] N. Kikuchi and J. Horbach, Europhys. Lett. **77**, 26001 (2007).
[20] G. Salin and D. Gilles, J. Phys. A **39**, 4517 (2006).
[21] H. Löwen, J. Phys.: Condens. Matter **4**, 10105 (1992).
[22] R. Messina and H. Löwen, Phys. Rev. Lett. **91**, 146101 (2003).
[23] P. Hartmann, G. J. Kalman, and K. K. Z. Donko, Phys. Rev. E **72**, 026409 (2005).
[24] P. Hartmann, G. Z. Kalman, and Z. Donko, J. Phys. A **39**, 4485 (2006).
[25] K. Nelissen, B. Partoens, and F. M. Peeters, Europhys. Lett. **79**, 66001 (2007).
[26] B. Liu and J. Goree, Phys. Rev. E **75**, 016405 (2007).
[27] A. Libal, C. Reichhardt, and C. J. O. Reichhardt, Phys. Rev. E **75**, 011403 (2007).
[28] G. J. Kalman, P. Hartmann, Z. Donko, and M. Rosenberg, Phys. Rev. Lett. **92**, 065001 (2004).
[29] B. Liu and J. Goree, Phys. Rev. Lett. **94**, 185002 (2005).
[30] J. M. Mendez-Alcaraz, M. Chavez-Paez, B. D'Aguanno, and R. Klein, Physica A **220**, 173 (1995).
[31] J. J. Gray and R. T. Bonnecaze, Langmuir **17**, 7935 (2001).
[32] A. Wysocki and H. Löwen, J. Phys.: Condens. Matter **16**, 7209 (2004).
[33] J. Dzubiella, G. P. Hoffmann, and H. Löwen, Phys. Rev. E **65**, 021402 (2002).
[34] E. Allahyarov, H. Löwen, and S. Trigger, Phys. Rev. E **57**, 5818 (1998).
[35] O. S. Vaulina and I. E. Dranzhevskii, Plasma Phys. Rep. **33**, 494 (2007).
[36] C. A. Murray and D. H. van Winkle, Phys. Rev. Lett. **58**, 1200 (1987).
[37] M. Brunner, C. Bechinger, W. Strepp, and V. Lobaskin, Europhys. Lett. **58**, 926 (2002).
[38] A. B. Fontecha, H. J. Schöpe, H. König, T. Palberg, R. Messina, and H. Löwen, J. Phys.: Condens. Matter **17**, S2779 (2005).
[39] E. Chang and D. Hone, Europhys. Lett. **5**, 635 (1988).
[40] E. Allahyarov, I. D'Amico, and H. Löwen, Phys. Rev. E **60**, 3199 (1999).
[41] M. E. Leunissen, C. G. Christova, A. P. Hynninen, C. P. Royall, A. I. Campbell, A. Imhof, M. Dijkstra, R. van Roij, and A. van Blaaderen, Nature (London) **437**, 235 (2005).
[42] A. P. Hynninen, C. G. Christova, R. van Roij, A. van Blaaderen, and M. Dijkstra, Phys. Rev. Lett. **96**, 138308 (2006).
[43] C. A. Murray and D. G. Grier, Annu. Rev. Phys. Chem. **47**, 421 (1996).
[44] However, intrinsic charge polydispersity has to be small enough in order to keep the charge distribution bimodal.
[45] C. R. Nugent, H. N. P. K. V. Edmond, and E. R. Weeks, Phys. Rev. Lett. **99**, 025702 (2007).
[46] N. Hoffmann, F. Ebert, C. N. Likos, G. Maret, and H. Löwen, Phys. Rev. Lett. **97**, 078301 (2006).
[47] M. H. Kong, B. Partoens, and F. M. Peeters, New J. Phys. **5**, 23 (2003).
[48] G. P. Hoffmann and H. Löwen, J. Phys.: Condens. Matter **12**, 7359 (2000).
[49] V. Nosenko, S. Nunomura, and J. Goree, Phys. Rev. Lett. **88**, 215002 (2002).
[50] V. Nosenko, J. Goree, Z. W. Ma, D. H. E. Dubin, and A. Piel, Phys. Rev. E **68**, 056409 (2003).
[51] H. Totsuji, T. Kishimoto, C. Totsuji, and T. Sasabe, Phys. Rev. E **58**, 7831 (1998).
[52] L. Messe, S. M. Clarke, T. Arnold, C. Dong, R. K. Thomas, and A. Inaba, Langmuir **18**, 4010 (2002).
[53] L. Messe, S. M. Clarke, C. Dong, R. K. Thomas, A. Inaba, M. D. Alba, and M. A. Castro, Langmuir **18**, 9429 (2002).
[54] S. M. Clarke, L. Messe, J. Adams, A. Inaba, T. Arnold, and R. K. Thomas, Chem. Phys. Lett. **373**, 480 (2003).
[55] V. N. Manoharan, T. Elsesser, and D. J. Pine, Science **301**, 483 (2003).
[56] J. Kecht, B. Mihailova, K. Karaghiosoff, S. Mintova, and T. Bein, Langmuir **20**, 5271 (2004).
[57] F. Yan and W. A. Goedel, Chem. Mater. **16**, 1622 (2004).
[58] A. E. Saunders and B. A. Korgel, ChemPhysChem **6**, 61 (2005).
[59] There is a trivial $Z \leftrightarrow 1/Z$ symmetry upon which one can safely reduce the phase diagram to $Z > 1$.
[60] B. D'Aguanno, R. Krause, J. M. Mendez-Alcaraz, and R. Klein, J. Phys.: Condens. Matter **4**, 3077 (1992).
[61] O. S. Vaulina, O. F. Petrov, A. V. Gavrikov, and V. E. Fortov, Plasma Phys. Rep. **33**, 278 (2007).
[62] For a confined colloidal suspension, p is the total lateral osmotic pressure of the colloids.
[63] L. Bonsall and A. A. Maradudin, Phys. Rev. B **15**, 1959 (1977).
[64] H. Löwen, J. N. Roux, and J. P. Hansen, J. Phys.: Condens. Matter **3**, 997 (1991).
[65] For a recent review, see G. E. Morfill, V. N. Tsytovich, H. Thomas, and S. V. Vladimirov, *Elementary Physics of Complex Plasmas* (Springer-Verlag, Berlin, 2008).
[66] P. N. Pusey and W. van Megen, Phys. Rev. Lett. **59**, 2083 (1987).
[67] H. N. W. Lekkerkerker, W. C. K. Poon, P. N. Pusey, A. Stroobants, and P. B. Warren, Europhys. Lett. **20**, 559 (1992).
[68] T. Hamanaka and A. Onuki, Phys. Rev. E **74**, 011506 (2006).
[69] T. Kawasaki, T. Araki, and H. Tanaka, Phys. Rev. Lett. **99**, 215701 (2007).
[70] J. Lekner, Physica A **157**, 826 (1989).
[71] M. Mazars, Mol. Phys. **105**, 1927 (2007).